

Optical and Dielectric studies in zirconium(IV) tungstate nanoparticles prepared by chemical co-precipitation method

Manoj Sadanandan, Beena Bhaskaran *

Department of Chemistry, D. B College, Sasthamcotta, Kollam, Kerala, India

* *E-mail: beenadbc@gmail.com*

Received 01 October 2011

Received in revised form 13 April 2012

Accepted 25 June 2012

Nanoparticles of zirconium(IV) tungstate are prepared by chemical co-precipitation method. The characterizations have been carried out by TG/DTA, DSC, AFM, XRD, FTIR and UV-Vis spectrum. PL spectrum shows two emission bands at 350 nm and at 477 nm. The effects of frequency on the dielectric behavior and ac electrical conductivity have been studied. The dielectric constant is found to be 119.43 at 1MHz. The ac conductivity is 7.29×10^{-8} S/cm.

Keywords: Zirconium(IV) tungstate; AFM; Optical band gap; ac conductivity; dielectric constant

1. INTRODUCTION

Low dimensional nanostructured materials are of great interest due to their unique physical and chemical properties [1]. These materials are considered as a bridge between the bulk and atomic or molecular structures. The size dependant properties of nanomaterials make them interesting and technologically important. Quantum confinement in semiconductor particles and surface plasmon resonance (SPR) in certain metal particles are some examples of size dependant properties [2]. Nanomaterials based on metals and semiconductors are the subject of extensive investigations because of their i) accessibility through a wide range of fabrication routes ii) unique characteristics and attributes and iii) extensive application potential [3]. Since the performances of devices based on these materials depend on the purity, size, shape and structure of the material, the preparation of nanoparticles with desired quality and low cost by convenient method is of great importance [4,5,6]. The dielectric and magnetic properties of oxides depend considerably on the size and shape of the particles [7]. Nanodielectrics, is the subject of study related to dielectric phenomena of nanoscopic materials having morphology of particles, sheets, wires and tubes etc. The area of nanodielectrics is relatively unexplored, but there is enormous scope to use nanomaterials in power electronic industry and as gate electrodes in thin film transistors [8].

Inorganic ion exchangers belonging to the class of Tetravalent Metal Acid (TMA) salts have the general formula $M(IV)(HXO_4)_2 \cdot nH_2O$, where $M(IV) = Zr, Ti, Th, Ce, Sn$, and $X = P, Mo, W$, etc. These compounds possess surface hydroxyl groups and the protons contained in this structural hydroxyl groups can be exchanged with several cations and thus these materials behave as cation exchangers and ion conductors [9,10]. In the present study, ac conductivity and dielectric properties of nanoparticles of zirconium(IV) tungstate belonging to the class of TMA salts prepared by chemical co-precipitation method is studied.

2. EXPERIMENTAL

2.1. Preparation of zirconium(IV) tungstate(ZW) nanoparticles

Nanoparticles of zirconium(IV) tungstate have been prepared by chemical co-precipitation method [11]. In a typical experiment, to a 250mL conical flask containing 25mL 0.02M EDTA, 25mL of 0.2M zirconium oxychloride solution was added from a burette with constant stirring using a magnetic stirrer in order to obtain a homogeneous metal ion solution. To this, 50mL of 0.2M sodium tungstate was added drop by drop very slowly. After the addition of sodium tungstate, the pH of the solution was adjusted to ~1 by adding 0.1M HCl. The resulting reaction mixture was then stirred for two hours. The gel so obtained was separated, washed with distilled water and dried.

2.2. Characterization

The thermogram of the sample was recorded on a Shimadzu Thermal Analyzer at a heating rate of 10°C/min. DSC of the material was taken using METTLER TOLEDO DSC 822e. AFM of the material was taken using NTEGRA (NT MDT) NSG 10. X-ray diffractograms ($2\theta=10-90^\circ$) were obtained on XPERT-PRO powder diffractometer with Cu-K α radiation. The FTIR spectrum was recorded using KBr wafer on the Thermo Nicolet FTIR model AVATAR 370 DTGS. The absorption spectra were recorded at room temperature using SHIMADZU UV-2550 UV Visible spectrophotometer. The photoluminescence measurement is carried out using Varian Cary Eclipse fluorescence spectrophotometer using xenon arc flash lamp as the excitation source. The dielectric permittivity measurement on the pellet of zirconium(IV) tungstate was carried out using HIOKI 3532-50 LCR Hi Tester in the frequency range 316Hz to 3.16MHz.

3. RESULTS AND DISCUSSION

The nanoparticles of ZW were obtained as white powder insoluble in acids and alkalis. TG/DTA of ZW is shown in Fig.1. TG shows i) 20.21% weight loss up to 100°C due to the loss of moisture/hydrated water ii) a gradual weight loss up to about 600°C, due to the condensation of structural hydroxyl groups as water molecules. The corresponding DTA curve shows an endothermic peak ~60°C. Above 450°C, several consecutive endothermic and exothermic processes occur due to the loss of surface hydroxyl groups as water molecules and formation of oxides along with some phase changes. The DSC of ZW is shown in Fig.2 and it constitutes one endothermic peak corresponding to the condensation of structural hydroxyl groups. The AFM picture of the sample is shown in Fig.3. It confirms the presence of nanosized particles of 14nm size. XRD spectra of as prepared and annealed samples of ZW are shown in Fig.4a and 4b respectively. From this, the average crystallite size of the powders were determined by using Scherrer's formula,

$$D = 0.9\lambda/\beta\cos\theta$$

where D is the average crystallite size in nm, λ the wavelength of X-ray radiation, θ the Bragg's angle and β the full width at half maximum of the peak observed for the sample [12]. The average size of the as prepared ZW was found to be 14nm which is in agreement with the data observed from AFM. From the XRD spectrum, it is found that the as prepared ZW is semicrystalline and as the annealing temperature increases crystallinity and particle size increases (Table I, Fig.4b). Above 700°C, the material is completely converted into crystalline form.

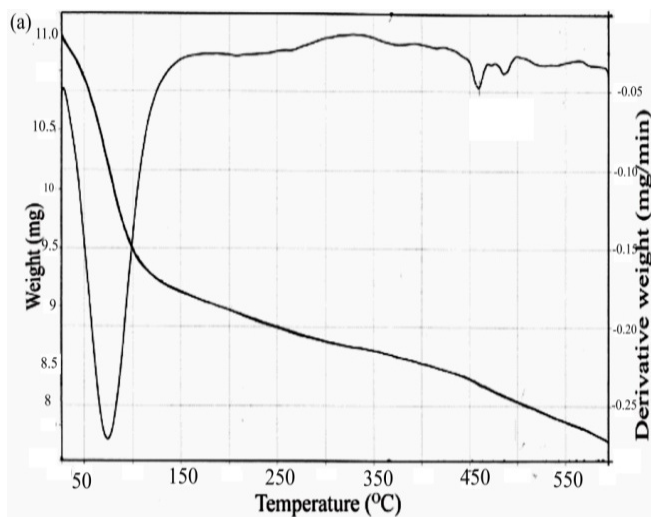


Fig. 1. TG/DTA of zirconium(IV) tungstate nanoparticles.

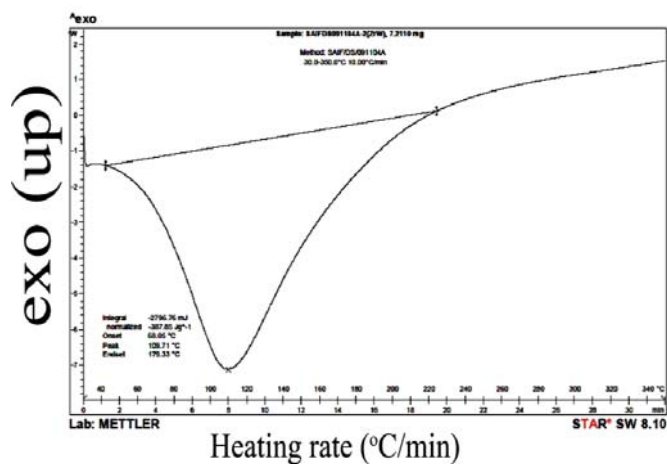


Fig. 2. DSC of zirconium(IV) tungstate nanoparticles.

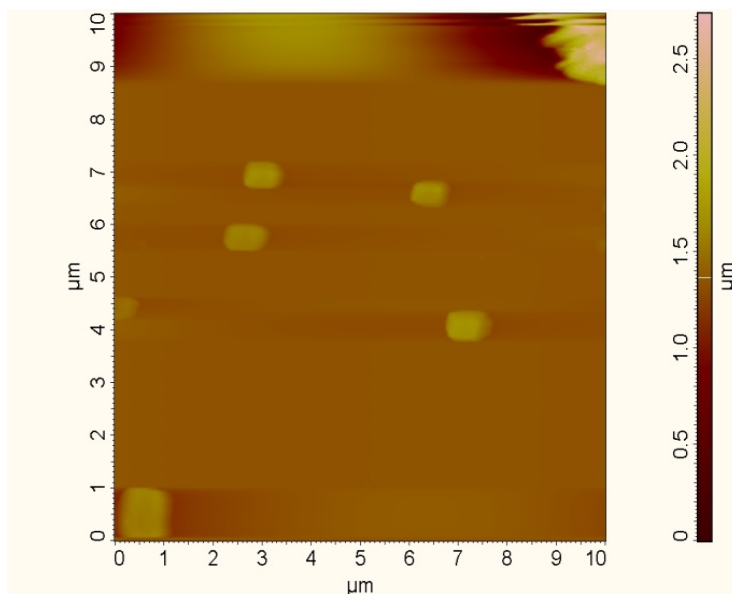


Fig. 3. AFM of zirconium(IV) tungstate nanoparticles.

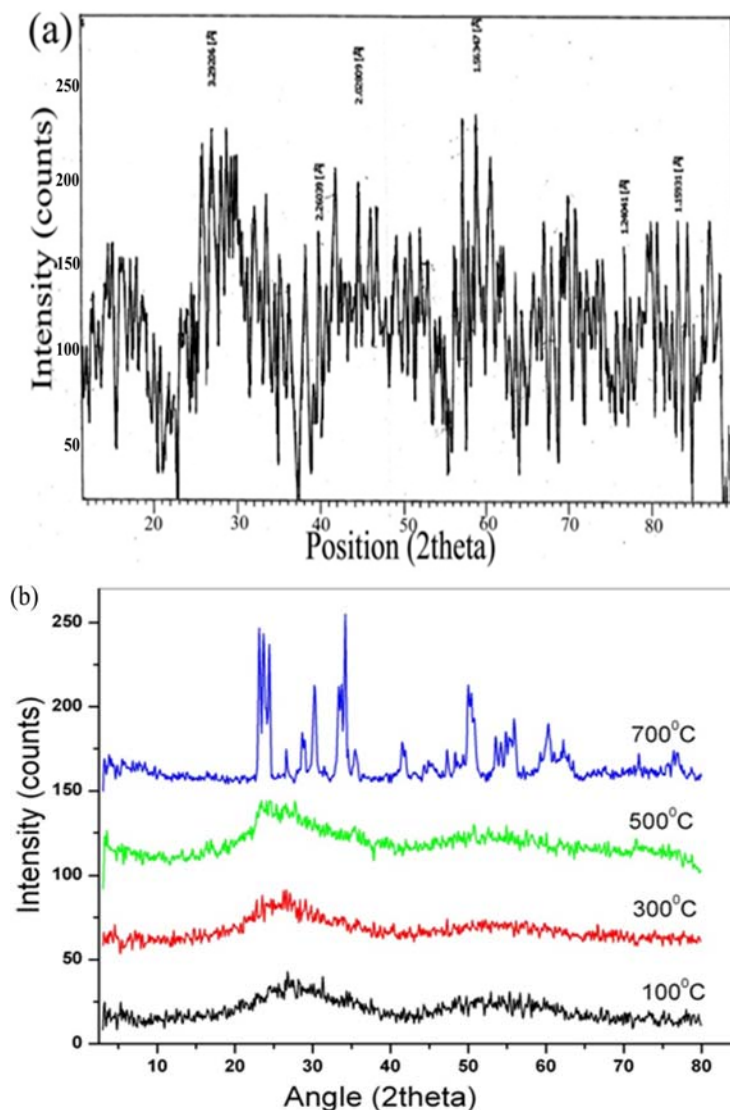


Fig. 4. XRD spectrum of (a) as prepared ZW and (b) ZW annealed at different temperatures.

Table I. Optical parameters and the particle size for as prepared ZW and for ZW annealed at different temperature.

Samples	Particle size (nm)	λ_{max} (nm)	$E_g(\lambda_{max})$ (eV)	$E_g(Tauc)$ (eV)	Eu (eV)
ZW(RT)*	14	260	4.70	4.48	2.47
ZW 100°C	20	282	4.41	3.29	1.45
ZW 300°C	28	301	4.12	3.00	1.50
ZW 500°C	30	308	4.03	2.26	1.92
ZW 700°C	35	269	4.60	2.19	2.49

*RT-Room Temperature

FT-IR spectra of ZW and the annealed samples are shown in Fig.5. The room temperature spectrum shows bands in the region $\sim 3415\text{cm}^{-1}$ and $\sim 1637\text{cm}^{-1}$ due to the presence of adsorbed water molecules or surface hydroxyl groups. Bands in the region $\sim 711\text{cm}^{-1}$ and $\sim 493\text{cm}^{-1}$ are due to W-O and Zr-O stretching vibrations respectively [13,14]. The band at $\sim 960\text{cm}^{-1}$ confirms the polytungstate structure with tungsten in octahedral coordination. This band is shifted to lower wavenumber in all samples due to strong tungsten zirconia interaction [15]. The deformation mode

of water molecules bound to the surface at $\sim 1610\text{cm}^{-1}$ is totally absent after 300°C , confirming that the samples are fully dehydrated.

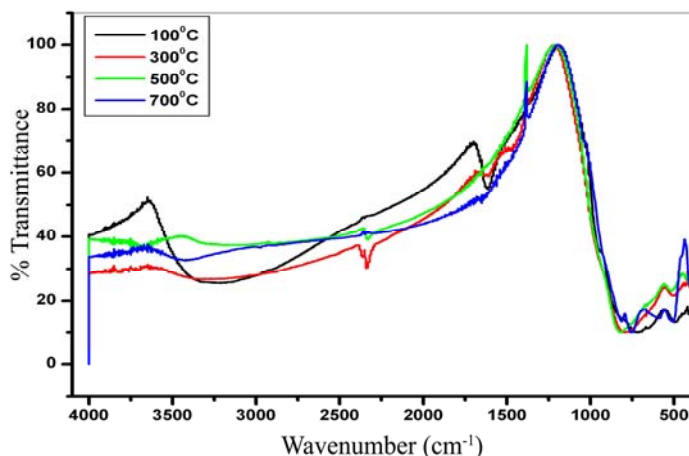


Fig. 5. FTIR spectrum of ZW at 100,300,500 and 7000C.

The UV/Vis spectra of the as prepared ZW and annealed samples are shown in Fig.6. UV spectrum gives information about excitonic or interband transition of nanomaterials. The fundamental absorption which corresponds to electron excitation from the valence band to the conduction band is used to determine the nature and value of the optical band gap. The relation between absorption coefficient, α , and the incident photon energy, $h\nu$, is given by the relation,

$$\alpha h\nu = A (h\nu - E_g)^n$$

where E_g is the band gap of the material, A is the absorption coefficient and the exponent n depends on the type of transition [16]. The value of band gap is determined by plotting $(\alpha h\nu)^{1/n}$ versus $h\nu$ and extrapolating the straight line portion to $h\nu$ axis (Fig.7). When the energy of the incident photon is less than the band gap, the increase in absorption coefficient is followed with an exponential decay of density of states of the localized band into the gap. The absorption edge here is called Urbach edge, α . Urbach energy characterizes the extend of the exponential tail of the absorption edge. The width of the Urbach tail is an indicator of defect levels in the forbidden gap. The following relation was used to calculate the Urbach tail, E_u .

$$\alpha(\nu) = \beta \exp(h\nu/E_u)$$

where β is a constant, E_u is the Urbach energy which indicates the width of the band tails of the localized states, h is the Plank's constant and ν the frequency of incident photons [17]. The natural logarithm of the absorption coefficient, $\alpha(\nu)$, was plotted as a function of the photon energy, $h\nu$ (Fig.8). The value of E_u was calculated by taking the reciprocal of the slopes of the linear portion in the lower photon energy region of curves. The exponential absorption tails, i.e. Urbach energy, depends on temperature, thermal vibrations in the lattice, induced disorder, static disorder, strong ionic bonds and on average photon energies [18]. λ_{max} , E_g calculated based on λ_{max} , E_g calculated based on Tauc relation and Urbach energy(E_u) calculated for ZW are listed in Table.I. It is found that the band gap decreases with increase in annealing temperature. The band gap has an inverse dependence on the grain size. It is also found that Urbach energy increases with increase in annealing temperature from 100° to 700°C and has direct dependence on particle size. The increase in Urbach energy with increase in annealing temperature suggests broadening of band tail width. Hence a large number of midgap states arises, increasing the conductivity and decreasing the band gap [19].

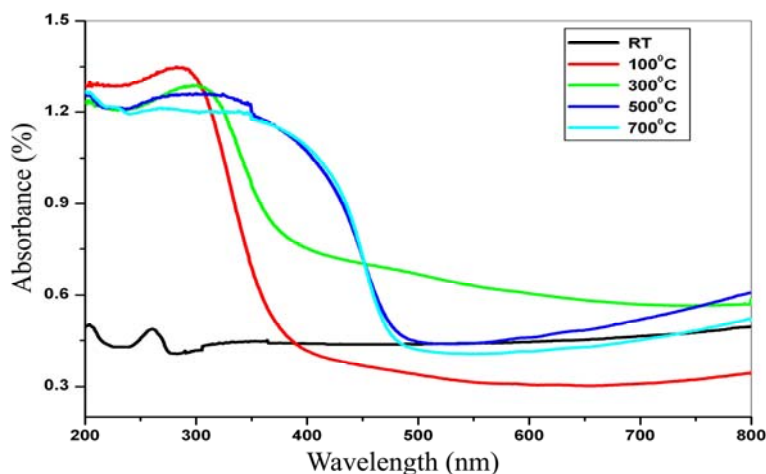


Fig. 6. Absorbance versus wavelength of as prepared ZW and for ZW annealed at different temperature.

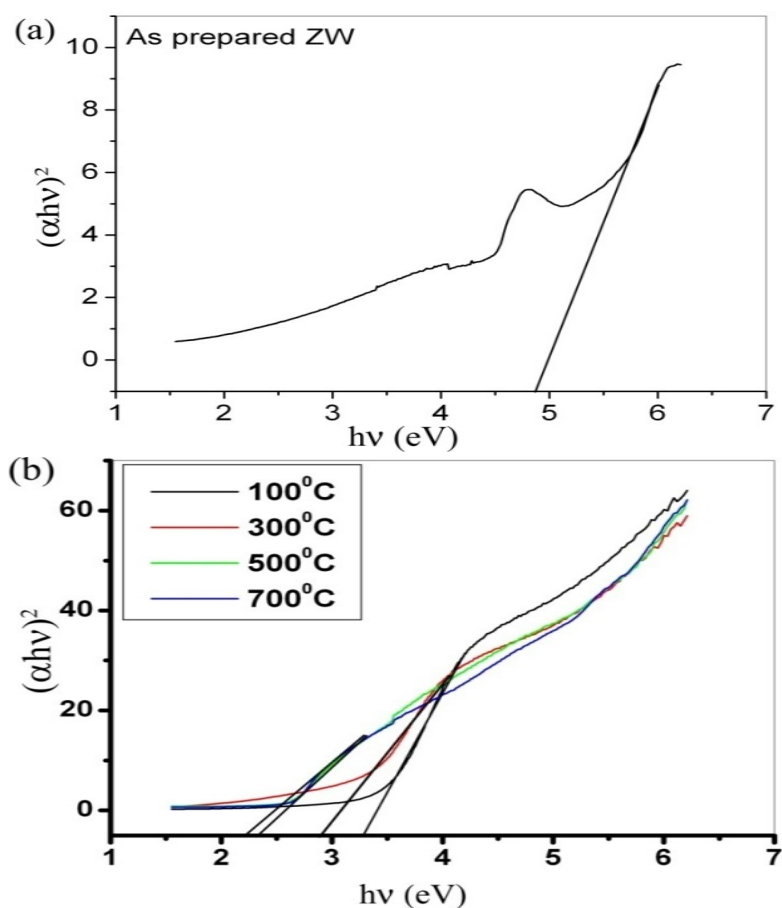


Fig. 7. $(\alpha h\nu)^2$ versus photon energy in eV (a) for as prepared ZW and (b) for ZW annealed at 100, 300, 500 and 700°C.

To investigate the optical properties of ZW, photoluminescence measurements were performed. From the emission spectrum (Fig.9), it is clearly found that there are two emission bands which peaked at 350 (UV band) and 477nm (blue band) respectively. These bands originate from the band edge radiative recombination and intrinsic defects present in the nanoparticles, mostly oxygen vacancy [20]. The edge emission is attributed to the excitonic transitions involving free excitons [21].

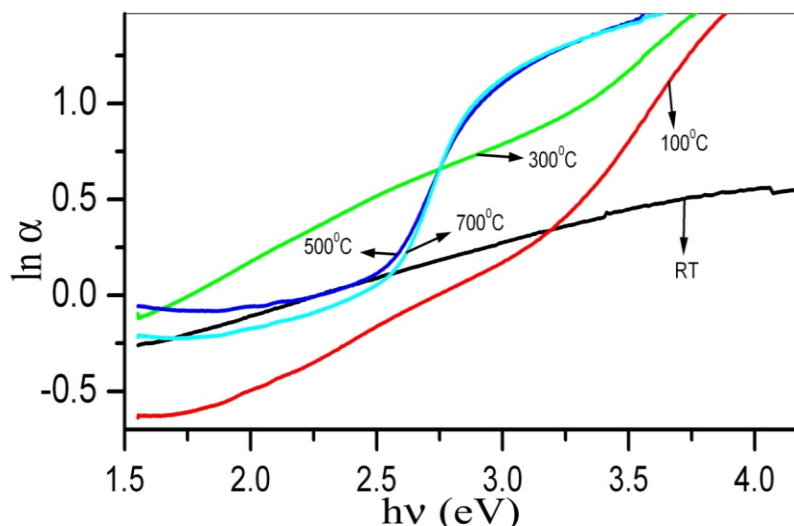


Fig. 8. The logarithm of the absorption coefficient, $\ln(\alpha)$, against photon energy in eV.

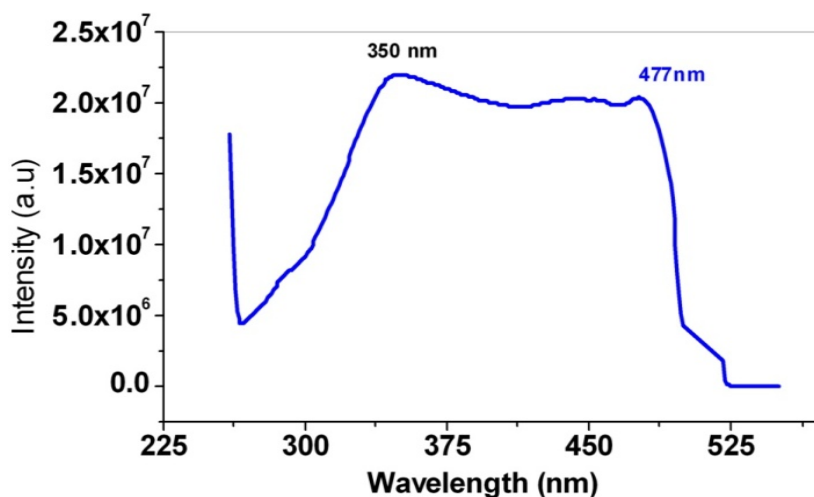


Fig. 9. Photoluminescence spectrum of ZW nanoparticles.

The variation of dielectric constant as a function of log frequency for as prepared ZW is shown in Fig.10. The dielectric constant and loss observed for this material is 119.43 and 3.72 respectively. The large value of the dielectric constant may be due to the fact that the nanocrystalline grains behave as nanodipoles, under the application of voltage. As the grain size are nanometer ordered, the number of grains per unit volume increases and hence the dielectric constant increases [22]. From the dielectric studies, it is seen that with decreasing log frequency, the dielectric constant increases. According to theory, the dielectric behavior of nanostructured material is primarily due to different types of polarizations present in the material such as space-charge polarization and rotation direction polarization [23]. It has also been observed that there is no dispersion at high frequency range, i.e. the dielectric constant is almost constant. Fig.11 shows the variation of dielectric loss with frequency. The dielectric loss increases with increase in frequency and it reaches a maximum and then decreases.

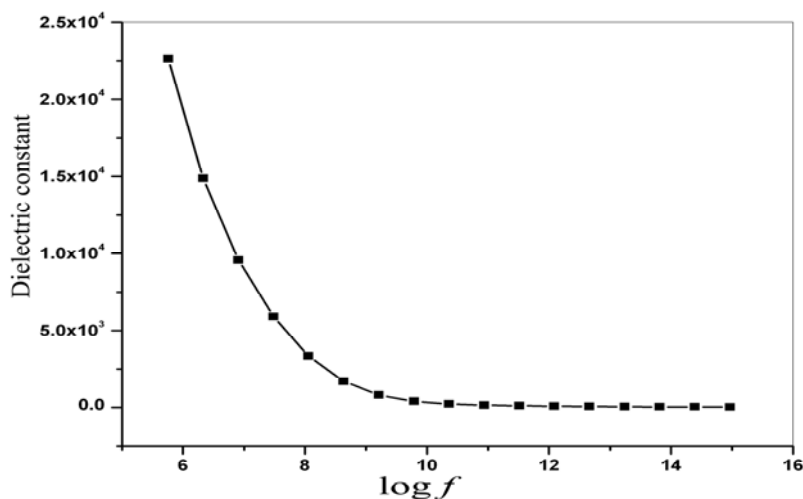


Fig. 10. Variation of dielectric constant with log frequency for ZW

The variations of capacitance and ac electrical conductivity with log frequency are shown in Fig.12 and 13 respectively. The capacitance decreases with increase in frequency and it remains almost constant at higher frequencies. Decrease in the value of capacitance with increase in frequency is due to the screening of the electric field by charge redistribution. It is seen that as frequency increases conductivity also increases. This can be explained by Correlated Barrier Hopping (CBH) [24]. Since tungsten exist in different valence state, W^{6+} , W^{5+} and W^{4+} , hopping of electron takes place between W^{6+} and W^{5+} and leads to high conductivity in this compound [25,26].

The conductivity of the present material is $7.29 \times 10^{-8} S/cm$. High surface to volume ratio of nanomaterials results in an increased surface defect density. These surface defect centers act as localized centers responsible for hopping conduction of electrons. The increased surface defect density causes an increase in ac conductivity of the material. High dielectric constant allows smaller capacitive components, thus offering the opportunity to decrease the size of the electronic device [27].

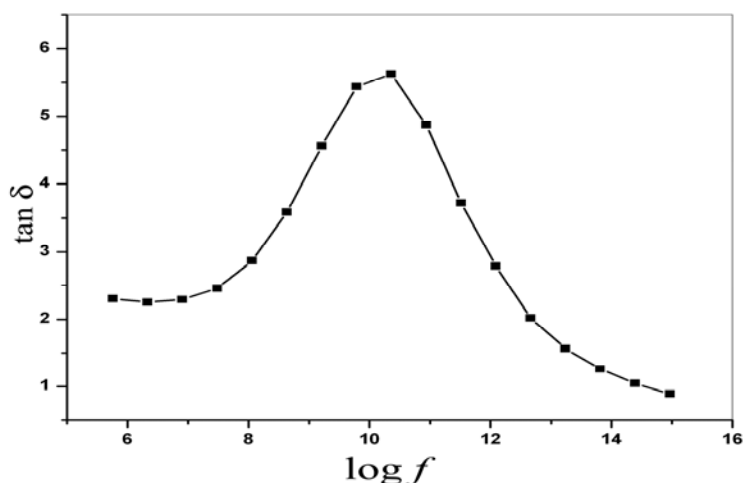


Fig. 11. Variation of loss with log frequency for ZW

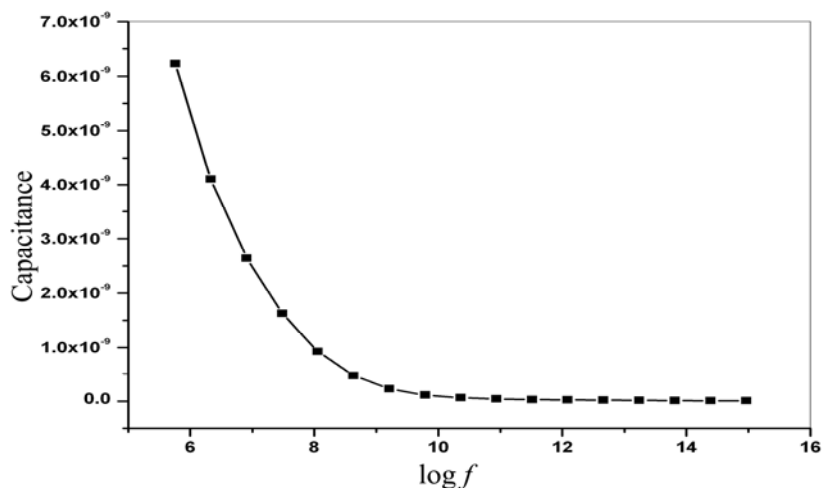


Fig. 12. Variation of capacitance with log frequency for ZW.

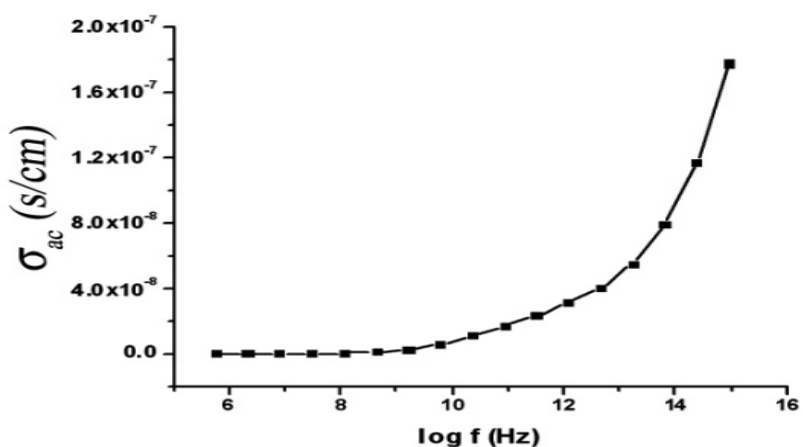


Fig. 13. Variation of ac conductivity with log frequency for ZW.

4. CONCLUSION

Thermal analysis of ZW shows that the material is stable up to fairly high temperature except for loss of surface hydroxyl group or occluded water molecules. XRD spectrum confirms that the as prepared ZW is semicrystalline and the material is completely converted into crystalline form at higher temperatures. As the annealing temperature increases, the particles agglomerate to big clusters thus increasing the particle size. AFM reveals that the particle size is 14nm. This result is in good agreement with the particle size calculated using Scherrer equation from the XRD data. From the FTIR spectrum, the major stretching and bending vibrations are identified. Optical absorption in the UV-Vis region indicates that ZW has direct band gap which decreases with increase in annealing temperature as well as grain size and varies from 4.48eV to 2.19eV. Optical absorption is also used to calculate the Urbach energy, which indicates disorder in ZW. The Urbach energy calculated for as prepared ZW is 2.47eV which suggests a broadening of band tail width and the presence of a large number of mid gap states which increase conductivity. ZW is also found to have a high value of dielectric constant which makes it suitable for microwave applications. This material is suitable for high frequency communication because of the low value of dielectric loss.

REFERENCES

- [1] Monika Gupta, Vidhika Sharma, Jaya Shrivastava, Anjana Solanki, A.P.Singh, V.R.Satsangi, S. Dass and Rohit Shrivastav, Bull.Mater.Sci., 32 (2009) 23-30.

- [2] T.S Sreeprasad, A.K Samal and T.Pradeep, *Bull.Mater.Sci.*, 31 (2008) 219-224.
- [3] A.Patra, K Rajesh and T.P.Radhakrishnan, *Bull.Mater.Sci.*, 31 (2008) 421-427.
- [4] Huazhi Wang, Xinli Kou, Jie Zhang and Jiangong Li, *Bull.Mater.Sci.*, 31(2008) 97-100.
- [5] H.T Zhang and X.H Chen, *Nanotechnology*, 17 (2006) 1384-1390.
- [6] M.Nidhin, R.Indumathy, K.J Sreeram and Balachandran Unni Nair, *Bull.Mater.Sci.*, 31(2008) 93-96.
- [7] Asok K.Ganguly, Sonalika Vaidya and Tokeer Ahmad, *Bull.Mater.Sci.*, 31 (2008) 415-419.
- [8] S.K Saha, *Bull.Mater.Sci.*, 31 (2008) 473-479.
- [9] Beena Pandit and Uma Chudasama, *Bull.Mater.Sci.*,24 (2001) 265-271.
- [10] Rakesh Thakkar, Heemanshu Patel and Uma Chudasama, *Bull.Mater.Sci.*, 30 (2007) 205-209 .
- [11] Manoj S and Beena B, *J.Nano- Electron Phys.*, 3(2011) 179-184.
- [12] Harol P Klug and Leroy E Alexander, *X-ray Powder Diffraction Procedure*, (John Wiley and Sons, New York), 1954.
- [13] Katabathini Narasimha Rao, Adapa Sridhar, Adam F. Lee, Stewart J Taveneer, Nigel A. Young and Karen Wilson, *Green Chem.* 8 (2006) 790-797.
- [14] Xuanyong Liu, Anping Huang, Chuanxian Ding and Paul K Chu, *Biomaterials*, 27 (2006) 3904-3911.
- [15] M.A Cortes-Jacome, J.A.Toledo, C.Angeles-Chavez, M.A.Guilar and J.A.Wang, *J.Phys.Chem.B*, 109 (2005) 22730-22739.
- [16] S.C Singh, R.K Swarnkar and R. Gopal, *Bull.Mater.Sci.*, 33 (2010) 21-26
- [17] F. Urbach, *Phys.Rev.* 92 (1953) 1324-1324.
- [18] M. Madani, *Bull.Mater.Sci.* 33 (2010) 65-73.
- [19] B.Pandey, P.P Pal, J Mukherjee, B. Das and A.K Kar, *Nanostructured Materials for Electronics, Energy and Environmental Applications*, (Macmillan, New Delhi) 2010.
- [20] S.K Nandi, S. Chakraborty, M.K Bera and C.K Maiti, *Bull.Mater.Sci.*, 30 (2007) 247-254.
- [21] D.G Thomas and J.J Hopfield, *Phys.Rev.* 128 (1962) 2135-2148.
- [22] P.K Gosh, M.K Mitra and K.K Chattopadhyay, *Nanotechnology*, 16 (2005) 107-112.
- [23] Nisha J.Tharayil, R Raveendran, Alexander Varghese Vaidyan and P.G.Chithra, *Indian J.Eng.Mater.Sci.*, 15 (2008) 489-496.
- [24] S.R Elliot, *Philos.Mag.*, 36 (1977) 1291-1296.
- [25] K.V Rao and A.Smakula, *J.App.Phys.*, 37 (1966) 319-323.
- [26] Xiuli Fu, Huilin Ge, Qin gkai Xing and Zhijian Peng, *Mater. Sci. and Eng. B*, 176 (2011) 926-931.
- [27] Alo Dutta, Chandrahas Bharti and T P Sinha, *Indian J.Eng.Mater.Sci.*,15 (2008) 181-186.